Research Article

Dynamic Response of Asymmetric and Nonlinear Packaging System under Random Excitation

Song-Ping Yang [ID] [1,2,3] **and Zhi-Wei Wang** [ID] [1,2,3]

[1]*Packaging Engineering Institute, Jinan University, Zhuhai 519070, China*
[2]*Key Laboratory of Product Packaging and Logistics of Guangdong Higher Education Institutes, Jinan University, Zhuhai 519070, China*
[3]*MOE Key Laboratory of Disaster Forecast and Control in Engineering, School of Mechanics and Construction Engineering, Jinan University, Guangzhou 510632, China*

Correspondence should be addressed to Zhi-Wei Wang; wangzw@jnu.edu.cn

This paper focuses on the dynamic response of three asymmetric and nonlinear packaging systems (ANPSs) of practical transport package under random excitation. Next to presenting the displacement probability density functions (PDFs) of ANPSs derived through FPK equations, the influences of the excitation grades and the characteristic parameters (such as the damping, the nonlinear stiffness, and the strain) of packaging cushion materials on the response are discussed in detail. Then, the generalized PDFs of the response peaks are defined and examined by three common distributions. The investigation shows that "inverse excitation cushion factors" (IECFs) have a significance on effecting the displacement PDFs approaching different distributions. Most PDFs of the unilateral response peaks approach Rayleigh distributions and present non-Gaussian characters. The present methods are verified through the validation numerical solutions. Furthermore, the application of the scheme for fatigue damage evaluation of the transport package is carried out.

1. Introduction

The spring-mass-damping system was introduced to describe transport package by Mindlin [1], who pioneered packaging dynamics study. The simplest package system was considered linear damping and linear stiffness; one of the biggest benefits of this was that you can use the superposition principle [2]. However, the packaging materials always follow nonlinear constitutive relations [3]. Peleg [4], Wang et al. [5], Wang and Hu [6], and Wang and Khan [7] did beneficial exploring on the packaging system with cubic nonlinear, tangent nonlinear, and tangent nonlinear stiffness under shock and vibration excitation, but the external excitation was always considered as deterministic harmonic excitation.

Since the external excitation during the transportation has always been random [8], an increasing effort was presently being expended to study the response of a spring-mass-damping packaging system under stochastic excitation [9–12]. Rountree et al. [13] studied the fragility of missile instrument under random vibration. Thakur et al. [14] established a nonlinear theoretical model for the packaging system to obtain displacement response under random vibration. Song [15] gave the definition of vibration fragility for the packaging system under random excitation and illustrated the difference with the impact fragility. Liaudet et al. [16] studied a random vibration model with fractional order stiffness and derived the probability density functions (PDFs) of displacement. Gan et al. [17] used the random average method to establish FPK equation for the packaging system with cubic nonlinear stiffness under stochastic excitation. Wang et al. [18] established a vibration model of the mass-spring-damping system by considering two stiffnesses of the system and the constraint condition under

acceleration random excitation in order to evaluate fatigue failure of the packaging paperboard box.

The scholars always consider nonlinear stiffness of the packaging system following the unidirectional function relation, such as cubic unidirectional function relation. However, due to the otherness of the packaging cushioning material or the asymmetries caused by packaging process, the stiffness of the packaging system presents asymmetric nonlinear characters.

Chen and Chen [19] discussed a single-degree-of-freedom (SDOF) damped system with the piecewise linear stiffness under Gaussian white noise. Zhuang et al. [20] explored the SDOF isolation system with the antisymmetrical and nonlinear stiffness, but only the approximate solution of the displacement mean square root was given by resolving the restoring force into odd function and even function. Fu et al. [21] obtained the response of a SDOF asymmetric piecewise linear system. Urbanik [22] studied the nonlinear vibration of the corrugated carton package through the piecewise nonlinear method. Yang et al. [23] used computer simulation to analyze the performance on the piecewise linear transit packaging system under oscillatory surroundings. Fang et al. [24, 25] introduced the SDOF nonlinear packaging oscillator with piecewise cubic nonlinearity, only obtained the joint displacement and velocity probability distribution. The systems with the piecewise asymmetric tangent or hyperbolic tangent stiffness under random excitation have seldom been investigated.

However, many packaging cushion materials such as the neoprene, preloading expandable polystyrene (EPS) foam, expandable polyethylene (EPE) foam, etc., follow tangent or hyperbolic tangent types of the force-displacement relation [1, 3, 26], and the cushion materials are around the product after packaging; the different materials sometimes are adopted as upper and lower layers cushioning material, so the piecewise asymmetric and nonlinear packaging systems (ANPSs) represent more accurate models of actual transport package.

Hence, this paper focuses on the dynamic response of asymmetric tangent nonlinear packaging system (ATNPS), asymmetric hyperbolic tangent nonlinear packaging system (AHNPS), and asymmetric tangent-hyperbolic tangent nonlinear packaging system (ATHNPS) under random excitation based on the FPK method which has been prospering as a method to obtain the system steady state solution [27, 28]. The study can be used as guidelines for first pass or fatigue damage evaluation of the transport package or the critical component.

The structure of this article is as follows. The transport package is modeled as ANPS in Section 2. In Section 3, the technology roadmap of numerical simulation process is illustrated. In Section 4, the response PDFs for three types of ANPSs under random excitation are derived through FPK equations, and the validation numerical models are carried out to verify the present method. Furthermore, the generalized peak PDFs are defined and examined by three common distributions. The influences of the system parameters, such as the damping correlation coefficient, the nonlinear stiffness, and the strain and the incentive intensity on the non-Gaussian characters of above

responses are analyzed in detail in Section 5. Section 6 gives the application of the scheme for fatigue evaluation. Finally, the main conclusions are summarized.

2. Vibration Model for Transport Package

During the logistics process, the complete transport package is subjected to the stochastic excitation in the horizontal or vertical direction while the gravity effect is always ignoring. The packaging cushion materials follow tangent or hyperbolic tangent types of the stress-deformation relations. Hence, the modeling for transport package regarding as SDOF ANPS is shown in Figure 1.

In Figure 1, m represents the mass of the product, δ represents the displacement of the product, and $f(\delta)$ and c represent the restoring force and the damping of packaging cushion materials, respectively. $f(\delta)$ follows relation of three types shown in Figure 2, showing the distinctions of ATNPS, AHTNPS, and ATHNPS.

Hence, the differential equation of motion for transport package can be written as

$$m\ddot{\delta} + c\dot{\delta} + f(\delta) = w(t), \tag{1}$$

where $w(t)$ represents the Gaussian white noise excitation with zero mean value. Letting $\alpha = (c/m)$, equation (1) can be written as

$$\ddot{\delta} + \alpha\dot{\delta} + \frac{f(\delta)}{m} = \frac{w(t)}{m}, \tag{2}$$

where $(w(t)/m) = 2\pi K$ and K represents the power spectral density of the excitation $w(t)$. $p(\delta, \dot{\delta})$ can be obtained through the Fokker–Planck equation [19]

$$p(\delta, \dot{\delta}) = C\exp\left[-\left\{\frac{\alpha}{\sigma_0^2}\left(\frac{\dot{\delta}^2}{2} + \int_0^\delta (f(\xi))d\xi\right)\right\}\right], \tag{3}$$

where $\sigma_0^2 = \pi K$ and the normalizing constant $C = [\int_{-\infty}^{+\infty}\int_{-\infty}^{+\infty} p(\delta, \dot{\delta})d\delta d\dot{\delta}]^{-1}$.

3. Numerical Verification

In order to verify the theoretical solution, the numerical simulation is conducted based on the following steps. Firstly, the Gaussian white noise excitation is conducted by digital simulation, and the excitation intensity $2\pi K$ is corresponding with the theoretical motivation. Secondly, through the four-stage Runge–Kutta method, the response of the packaging system characterized by digital simulation can also be obtained. The piecewise programs are considering in Runge–Kutta calculation steps. Thirdly, the Monte Carlo approach, which was first proposed by Metropolis et al. [29] and generalized by Hastings [30], is used to solve complex integrals [31]. The technology roadmap of numerical simulation process is shown in Figure 3, and afterwards the comparisons between the theoretical solution and numerical result can be given.
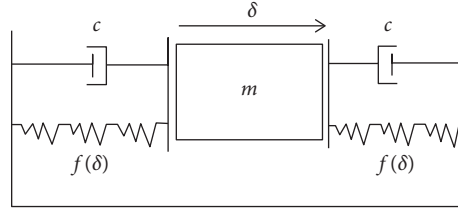
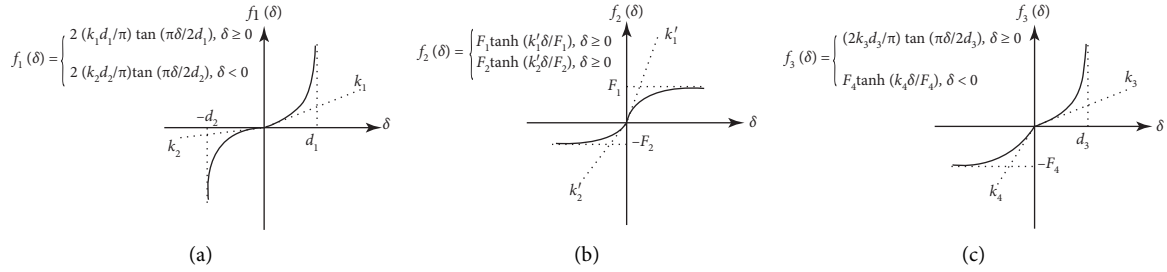FIGURE 1: The proposed vibration model for transport package.

(a)

(b)

(c)

FIGURE 2: Three types of restoring forces of packaging cushion materials. (a) Antisymmetry tangent type. (b) Antisymmetry hyperbolic tangent type. (c) Asymmetric tangent-hyperbolic tangent type.
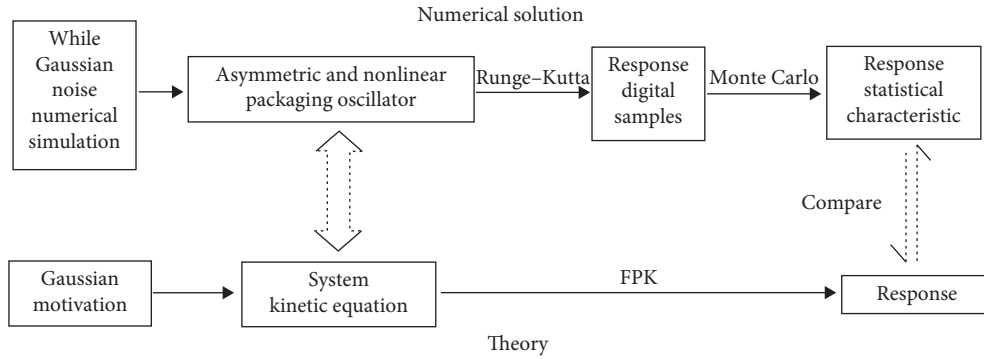

FIGURE 3: Technology roadmap of numerical verification.

4. Response PDFs of ANPSs

Three packaging systems are concerned with the different piecewise forms of stiffnesses. They can be expressed as three forms of restoring forces. PDFs of the displacement and velocity for three systems are investigated.

4.1. Response PDFs of ATNPS. Some packaging cushion materials follow tangent force-displacement relation, so the nonlinear restoring force of ATNPS considering the asymmetric tangent stiffness is as follows:

$$
f_1(\delta) = \begin{cases} 2\dfrac{k_1 d_1}{\pi}\tan\dfrac{\pi\delta}{2d_1}, & \delta \geq 0, \\[3mm] 2\dfrac{k_2 d_2}{\pi}\tan\dfrac{\pi\delta}{2d_2}, & \delta < 0, \end{cases} \tag{4}
$$

and letting $(k_1/m) = \omega_1^2$ and $(k_2/m) = \omega_2^2$ and substituting equation (4) into (3) result in

$$
p_1(\delta,\dot\delta) = \begin{cases} C\exp\left[-\dfrac{\alpha}{\sigma_0^2}\left(\dfrac{\dot\delta^2}{2} - \dfrac{4\omega_1^2}{\pi^2}d_1^2 \cdot \ln\cos\dfrac{\pi\delta}{2d_1}\right)\right], & 0 \leq \delta < d_1, \\[4mm] C\exp\left[-\dfrac{\alpha}{\sigma_0^2}\left(\dfrac{\dot\delta^2}{2} - \dfrac{4\omega_2^2}{\pi^2}d_2^2 \cdot \ln\cos\dfrac{\pi\delta}{2d_2}\right)\right], & -d_2 < \delta < 0. \end{cases}
$$

$$(5)$$

Assuming $\sigma_0^2 = 0.1, \alpha = 0.5$, $\omega_1 = 1, d_1 = 2, \omega_2 = 2$, and $d_2 = 4$, the joint PDF of the displacement and velocity $p_1(\delta,\dot\delta)$ of ATNPS is obtained to compare with numerical result shown in Figure 4. Both have the nearly same shape and peak, leading to the verification of the theory.

The displacement PDF of ATNPS can also be given through the Fokker–Planck equation.
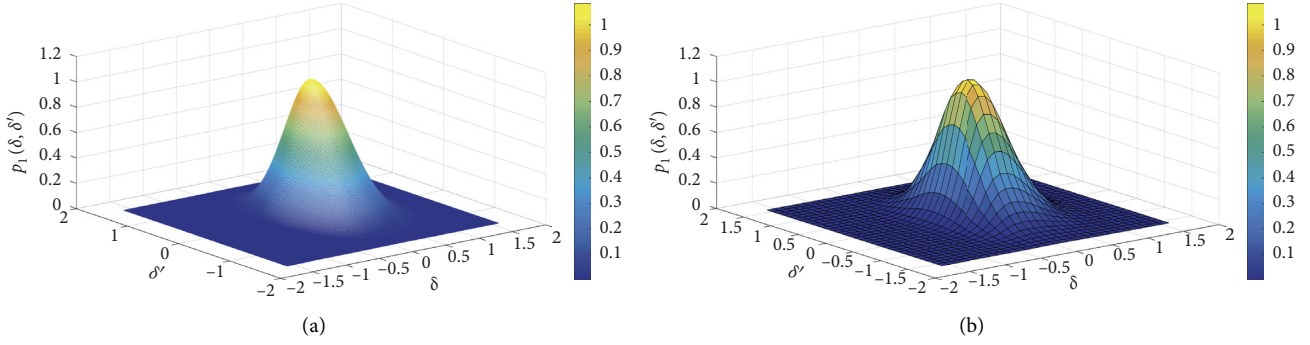
FIGURE 4: Comparison of joint PDF of the displacement and velocity of ATNPO. (a) Theoretical solution. (b) Numerical solution.

$$p_1(\delta) = \begin{cases} C_1 \exp\left[\dfrac{\alpha}{\sigma_0^2}\left(\dfrac{4\omega_1^2}{\pi^2}d_1^2 \cdot \ln\cos\dfrac{\pi\delta}{2d_1}\right)\right], & 0 \le \delta < d_1, \\[4mm] C_1 \exp\left[\dfrac{\alpha}{\sigma_0^2}\left(\dfrac{4\omega_2^2}{\pi^2}d_2^2 \cdot \ln\cos\dfrac{\pi\delta}{2d_2}\right)\right], & -d_2 < \delta < 0, \end{cases} \tag{6}$$

where the normalizing constant $C_1 = [\int_{-\infty}^{+\infty} p_1(\delta)d\delta]^{-1}$. In order for examining the influences of the external excitation and the system parameters, such as the damping correlation coefficient, the nonlinear stiffness, and the strain on the response, the figures are plotted of different characteristic parameters.

Letting $\alpha = 0.5, \omega_1 = 1, d_1 = 2, \omega_2 = 2,$ and $d_2 = 4,$ the displacement PDFs of ATNPS can be plotted for various values of σ_0^2 in Figure 5. That means the displacement response of the system only concerns with the external excitation grade. After comparing with the numerical solutions shown on the left, we use Gaussian distribution to examine $p_1(\delta)$ shown on the right of Figure 5.

We can see a good agreement is achieved between theoretical and numerical solution of $p_1(\delta)$ from Figure 5, leading to further verify the theoretical model. It can be seen that the displacements δ corresponding to the displacement PDF $p_1(\delta)$ of the product move higher and narrower with excitation level decreases. Meanwhile, the restoring force $f(\delta)$ of packaging cushion material gradually approaches the initial linear, and the response displacement is smaller so that the displacement PDF $p_1(\delta)$ approaches Gaussian distribution with the external excitation grade σ_0^2 decreases.

Figure 6 presents the displacement PDFs of ATNPS except the difference of the damping correlation coefficient α. As the cushion capacity of the system increases with the α increases, then the displacement responses of the product are limited to a smaller range, and the nonlinear factors can

be compensated in the system so that the displacement PDF $p_1(\delta)$ is closer to Gaussian distribution. It is interesting to find that as α tends to 0 (the system damping tends to 0), $p_1(\delta)$ approaches a uniform distribution.

Letting $\sigma_0^2 = 0.1, \alpha = 0.5, \omega_1 = 1,$ and $\omega_2 = 1,$ the displacement PDFs of ATNPS can be plotted for various values of the strains d_1 and d_2 of the packaging cushion materials in Figure 7. Letting d_1 equal to $d_2,$ with the d_1 and d_2 increase simultaneously, the displacement PDF $p_1(\delta)$ approaches Gaussian distributions. Otherwise, the displacement PDF $p_1(\delta)$ presents distinct non-Gaussian character. Displacement responses are limited to less than d_1 and d_2 because the nonlinear restoring force $f(\delta)$ of the system follows asymmetric tangent type with the boundary strain of d_1 and d_2.

Figure 8 shows the displacement PDFs of ATNPS for various ω_1 and ω_2 which represent the initial angular frequency of the packaging cushion material. $p_1(\delta)$ nearly follows Gaussian distribution when $\omega_1 = \omega_2$ because the asymmetric tangent nonlinear packaging system begins same deformation on the both sides. We also discover that $p_1(\delta)$ is symmetrical when ω_1 exchange $\omega_2.$

Letting $n_1 = (4\alpha\omega_1^2 d_1^2/\pi^2\sigma_0^2)$ and $n_2 = (4\alpha\omega_2^2 d_2^2/\pi^2\sigma_0^2),$ equation (6) becomes

$$p_1(\delta) = \begin{cases} C_1\left(\cos\dfrac{\pi\delta}{2d_1}\right)^{n_1}, & 0 \le \delta < d_1, n_1 \ge 0, \\[4mm] C_1\left(\cos\dfrac{\pi\delta}{2d_2}\right)^{n_2}, & -d_2 < \delta < 0, n_2 \ge 0. \end{cases} \tag{7}$$

When $d_1 = d_2 = 2,$ the amplitude δ is plotted versus displacement PDFs of ATNPS at various values of n_1 and n_2 in Figure 9. Because n_1 and n_2 are directly proportional to cushion performance parameters $\omega_1^2, d_1, \omega_2^2,$ and d_2 of packaging materials, they are inversely proportional to the measure of the excitation level $\sigma_0^2.$ Hence, n_1 and n_2 maybe called "inverse excitation cushion factors"
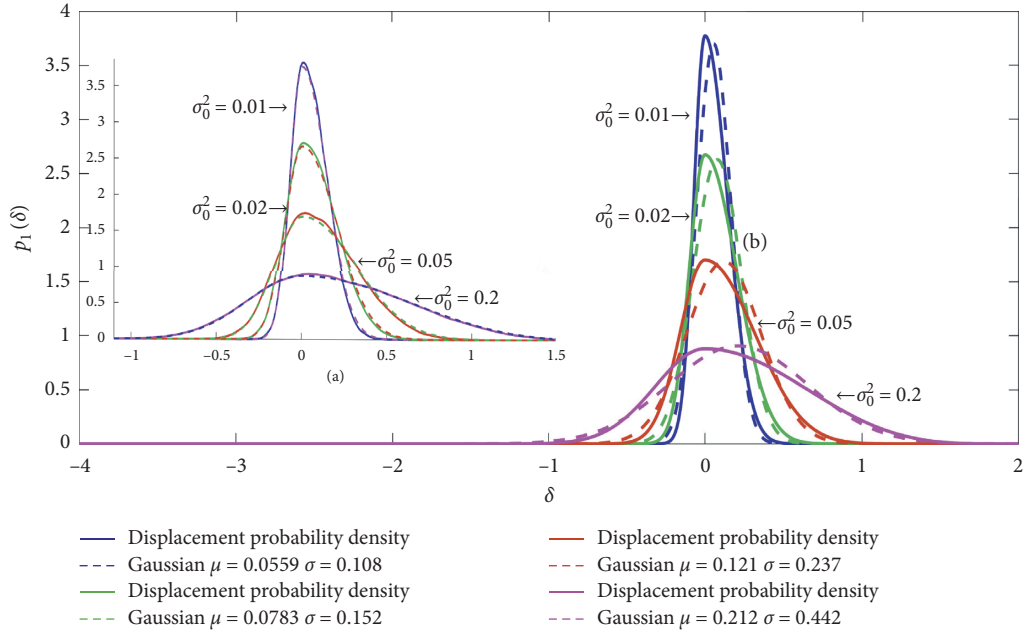
FIGURE 5: Displacement PDFs of ATNPS for various values of excitation grades. (a) Comparison of the numerical and theoretical solution. (b) The result of Gaussian fitting.
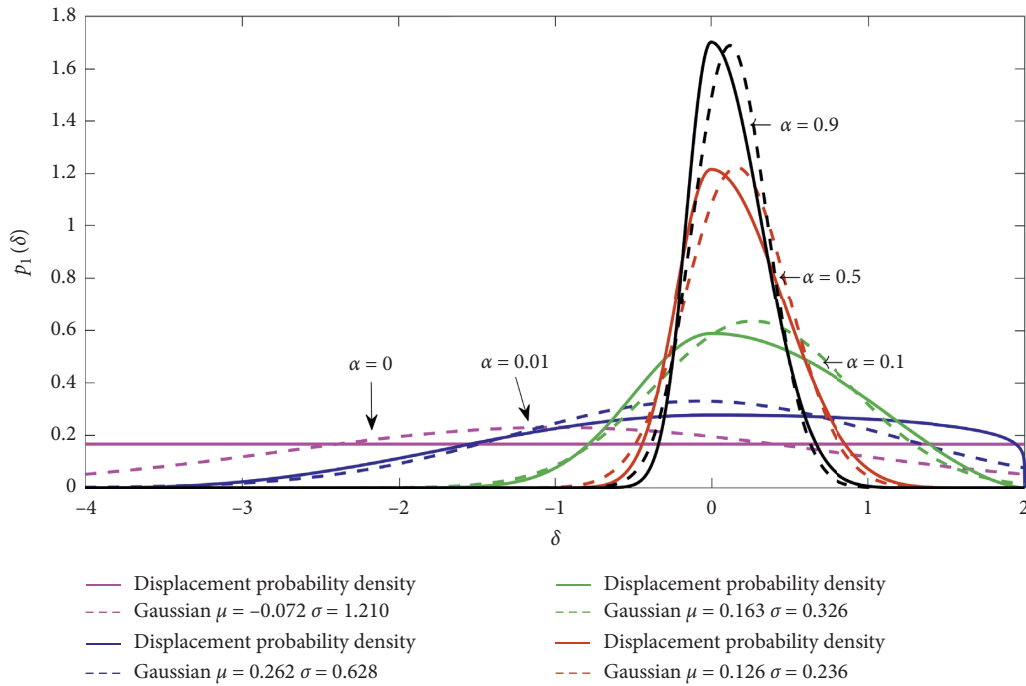

FIGURE 6: Displacement PDFs of ATNPS for different damping coefficients.

(IECFs). We find that as n_1 and n_2 tend to 0 (σ_0^2 tends to infinity), $p_1(\delta)$ approaches a uniform distribution. When n_1 and $n_2 < 9$, $p_1(\delta)$ presents non-Gaussian characters. It can be seen that as $n_1 = n_2 \geq 9$, $p_1(\delta)$ constantly approaches Gaussian distribution; as n_1 and n_2 tend to infinity (σ_0^2 tends to 0), $p_1(\delta)$ can be regarded as following Gaussian distribution.

$p_1(\delta)$ follows "piecewise cosine exponential distribution," so the normalizing constant C_1 can be obtained from

$$C_1 = \left[\int_{-\infty}^{+\infty} \int_{-\infty}^{+\infty} p(\delta, \dot{\delta}) \mathrm{d}\delta \mathrm{d}\dot{\delta} \right]^{-1}$$

$$= \left[\int_{-d_2}^{0} \left(\cos \frac{\pi\delta}{2d_2} \right)^{n_2} + \int_{0}^{d_1} \left(\cos \frac{\pi\delta}{2d_1} \right)^{n_1} \right]^{-1}, \tag{8}$$

letting $y = \cos(\pi\delta/2d)$ and $\int_{0}^{\pi/2} (\cos y)^n = \sqrt{\pi}/2\Gamma(n+1/2)/\Gamma(n/2+1)$ from the table of integrals [32], so
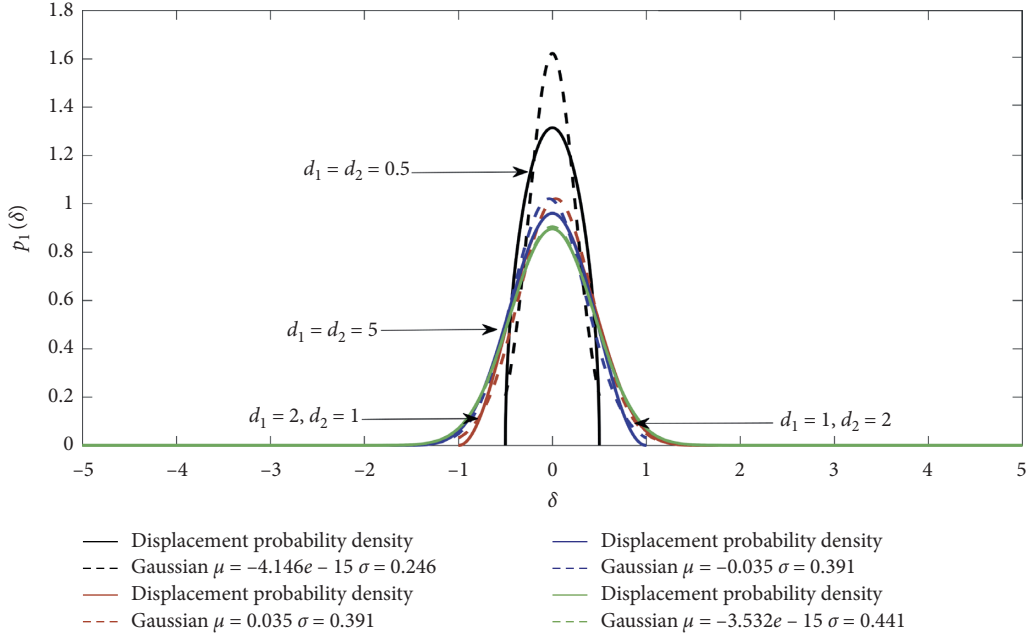
FIGURE 7: Displacement PDFs of ATNPS for various values of packaging material strains.

$$C_1 = \frac{\sqrt{\pi}}{[d_1\Gamma(n_1 + 1/2)/\Gamma(n_1/2 + 1) + d_2\Gamma(n_2 + 1/2)/\Gamma(n_2/2 + 1)]}, \quad n_1 \geq 0, n_2 \geq 0. \tag{9}$$

The mean-square response of the mass m or the variance of x is determined by $\sigma_\delta^2 = \int_{-\infty}^{\infty} \delta^2 p(\delta)\mathrm{d}\delta$.

4.2. Response PDFs of AHTNPS.

Due to some packaging cushion materials follow asymmetric hyperbolic tangent constitutive relation, the restoring force $f(\delta)$ of AHTNPS can be expressed as

$$f_2(\delta) = \begin{cases} F_1\tanh\dfrac{k_1'\delta}{F_1}, & \delta \geq 0, \\[3mm] F_2\tanh\dfrac{k_2'\delta}{F_2}, & \delta < 0, \end{cases} \tag{10}$$

and assuming $(F_1/m) = \omega_1'^2$ and $(F_2/m) = \omega_2'^2$, and then substituting equation (10) into (3), $p(\delta, \dot{\delta})$ can be obtained as

$$p_2(\delta, \dot{\delta}) = \begin{cases} C'\exp\left[-\dfrac{\alpha}{\sigma_0^2}\left(\dfrac{\dot{\delta}^2}{2} + \dfrac{F_1\omega_1'^2}{k_1'} \cdot \text{lncosh}\dfrac{k_1'\delta}{F_1}\right)\right], & \delta \geq 0, \\[4mm] C'\exp\left[-\dfrac{\alpha}{\sigma_0^2}\left(\dfrac{\dot{\delta}^2}{2} + \dfrac{F_2\omega_2'^2}{k_2'} \cdot \text{lncosh}\dfrac{k_2'\delta}{F_2}\right)\right], & \delta < 0. \end{cases} \tag{11}$$

When $\sigma_0^2 = 0.1, \alpha = 0.5, \omega_1 = 1, \omega_2 = 2, (k_1'/F_1) = 0.01$, and $(k_2'/F_2) = 0.02$, the displacement and velocity united PDF $p_2(\delta, \dot{\delta})$ of AHTNPS is shown in Figure 10. The

numerical model is also carried out and compared with the theoretical solution, leading to the verification of the theory.

The displacement PDF of AHTNPS can be obtained

$$p_2(\delta) = \begin{cases} C_1'\exp\left[-\dfrac{\alpha}{\sigma_0^2}\left(\dfrac{F_1\omega_1'^2}{k_1'} \cdot \text{lncosh}\dfrac{k_1'\delta}{F_1}\right)\right], & \delta \geq 0, \\[4mm] C_1'\exp\left[-\dfrac{\alpha}{\sigma_0^2}\left(\dfrac{F_2\omega_2'^2}{k_2'} \cdot \text{lncosh}\dfrac{k_2'\delta}{F_2}\right)\right], & \delta < 0, \end{cases} \tag{12}$$

where the normalizing constant $C_1' = [\int_{-\infty}^{+\infty} p_2(\delta)\mathrm{d}\delta]^{-1}$ can be calculated, as well; when $\alpha = 0.5, \omega_1' = 1, \omega_2' = 2, (k_1'/F_1) = 0.01$, and $(k_2'/F_2) = 0.02$, the displacement PDFs of AHTNPS can be plotted for various values of σ_0^2 representing the excitation grade in Figure 11. In comparison with the numerical solutions of the displacement PDFs of AHTNPS, leading to further verify the theoretical model, the displacements δ move lower and wider as the excitation intension increases.

Assuming $\sigma_0^2 = 0.1, \omega_1' = 1, \omega_2' = 2, (k_1'/F_1) = 0.01$, and $(k_2'/F_2) = 0.02$, Figure 12 depicts the displacement PDFs of AHTNPS with different α. As the cushion capacity of the system decreases with decrease in α the displacement response varies over a larger range, and the system damping is considered as linear, but the nonlinear stiffness factors were expended in the system, and $p_2(\delta)$ presents distinct non-Gaussian characters.
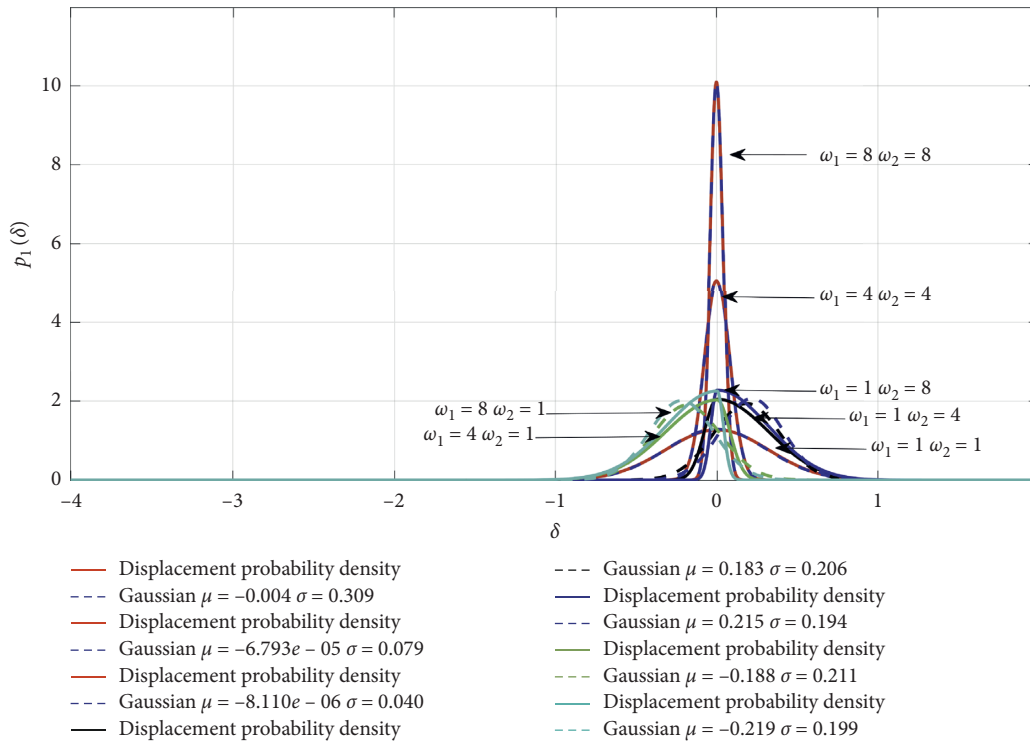
Figure 8: Displacement PDFs of ATNPS for various values of initial angular frequencies.
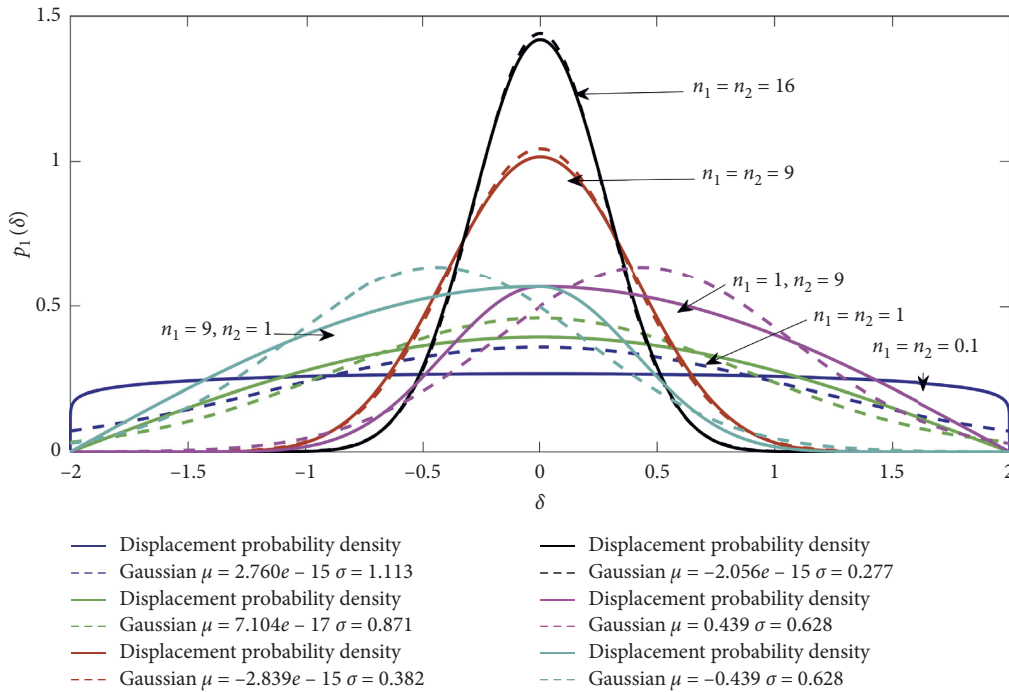

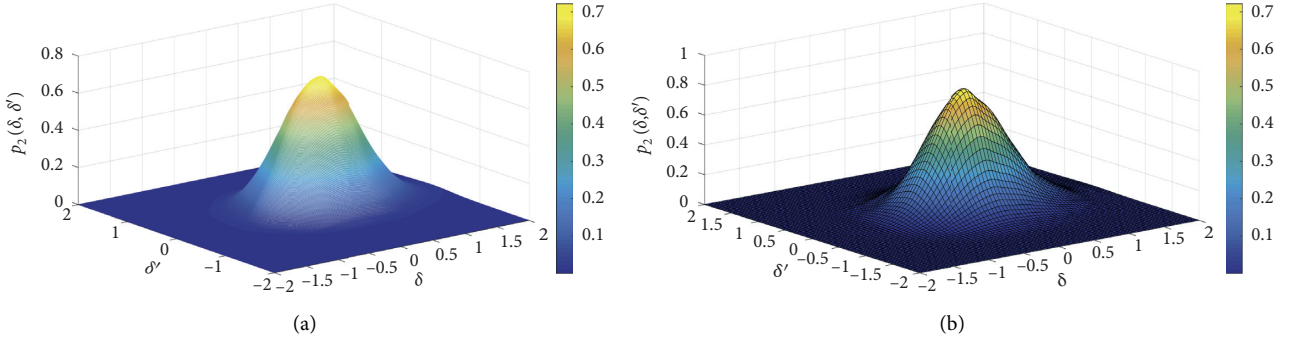Figure 9: Displacement PDFs of ATNPS for various values of IECFs.

FIGURE 10: Comparison of displacement and velocity united PDF of HATNPO. (a) Theoretical solution. (b) Numerical solution.

It is obvious that as α tends to 0 (the system damping tends to 0), $p_2(\delta)$ approaches a uniform distribution.

Letting $n_1' = (-\alpha F_1 \omega_1'^2 / k_1' \sigma_0^2)$ and $n_2' = (-\alpha F_2 \omega_2'^2 / k_2' \sigma_0^2)$, equation (12) becomes

$$
p_2(\delta) = \begin{cases} C_1' \left(\cosh \dfrac{k_1' \delta}{F_1} \right)^{n_1'}, & \delta \geq 0, n_1' \leq 0, \\[2mm] C_1' \left(\cosh \dfrac{k_2' \delta}{F_2} \right)^{n_2'}, & \delta < 0, n_2' \leq 0. \end{cases} \tag{13}
$$

When $(k_1'/F_1) = (k_2'/F_2) = 0.01$, the amplitudes are plotted versus displacement PDFs of AHTNPS for various values of n_1' and n_2' in Figure 13. It is interesting to find that as IECFs n_1' and n_2' tend to 0 (σ_0^2 tends to infinity), $p_2(\delta)$ approaches a uniform distribution. As n_1' and $n_2' < -3$, $p_2(\delta)$ presents non-Gaussian characters. It also clearly shows that as $n_1' = n_2' \geq -3$, $p_2(\delta)$ is gradually closer to Gaussian distribution, and as n_1' and n_2' tend to infinity (σ_0^2 tends to 0), $p_2(\delta)$ can be considered as Gaussian distribution.

4.3. Response PDFs of ATHNPS. Using the tangent and hyperbolic tangent type of packaging cushion materials together, the restoring force of ATHNPS can be expressed as

$$
f_3(\delta) = \begin{cases} 2\dfrac{k_3 d_3}{\pi} \tan \dfrac{\pi \delta}{2d_3}, & \delta \geq 0, \\[2mm] F_4 \tanh \dfrac{k_4 \delta}{F_4}, & \delta < 0, \end{cases} \tag{14}
$$

if $(k_3/m) = \omega_3^2$ and $(F_4/m) = \omega_4^2$, then substituting equation (14) into (3), $p(\delta, \dot{\delta})$ can be obtained

$$
p_3(\delta, \dot{\delta}) = \begin{cases} C'' \exp\left[-\dfrac{\alpha}{\sigma_0^2} \left(\dfrac{\dot{\delta}^2}{2} - \dfrac{4\omega_3^2}{\pi^2} d_3^2 \cdot \ln \cos \dfrac{\pi \delta}{2d_3} \right) \right], & 0 \leq \delta < d_3, \\[3mm] C'' \exp\left[-\dfrac{\alpha}{\sigma_0^2} \left(\dfrac{\dot{\delta}^2}{2} + \dfrac{F_4 \omega_4^2}{k_4} \cdot \ln \cosh \dfrac{k_4 \delta}{F_4} \right) \right], & \delta < 0. \end{cases}
$$

$$\tag{15}$$

When $\sigma_0^2 = 0.1, \alpha = 0.5, \omega_3 = 1, d_3 = 2, \omega_4 = 1$, and $(k_4/F_4) = 0.1$, the displacement and velocity united PDF $p_3(\delta, \dot{\delta})$ of ATHNPS is shown in Figure 14.

The numerical model is carried out, leading to the verification of the theory. The value of $p_3(\delta, \dot{\delta})$ with different δ and $\dot{\delta}$ is available because $p_3(\delta, \dot{\delta})$ is conducted by cos and cosh functions, and $p_3(\delta, \dot{\delta})$ is small percentage located on the side of $\delta < 0$ by the δ-axis and less distributed on the side of $\dot{\delta} < 0$ by the $\dot{\delta}$-axis.

The displacement PDF of ATHNPS can be expressed as

$$
p_3(\delta) = \begin{cases} C_1' \exp\left[\dfrac{\alpha}{\sigma_0^2} \left(\dfrac{4\omega_3^2 d_3^2}{\pi^2} \cdot \ln \cos \dfrac{\pi \delta}{2d_3} \right) \right], & 0 \leq \delta < d_3, \\[3mm] C_1' \exp\left[-\dfrac{\alpha}{\sigma_0^2} \left(\dfrac{F_4 \omega_4^2}{k_4} \cdot \ln \cosh \dfrac{k_4 \delta}{F_4} \right) \right], & \delta < 0, \end{cases}
$$

$$\tag{16}$$

where the normalizing constant $C_1' = [\int_{-\infty}^{+\infty} p_3(\delta) d\delta]^{-1}$. As $\alpha = 0.5, \omega_3 = 1, d_3 = 2, \omega_4 = 2$, and $(k_4/F_4) = 0.1$, the displacement PDFs of ATHNPS can be plotted for various values of σ_0^2 in Figure 15. It shows the regularity between the displacement response of ATHNPS and the different incentive intensity.

A good agreement is achieved between theoretical and numerical solutions of displacement PDFs of ATHNPS, leading to further verify the theoretical model. σ_0^2 is lower as the external excitation intensity decreases; we can see that the displacements δ corresponding to $p_3(\delta)$ of the product moves higher and narrower with excitation level decreases. Meanwhile, the restoring force $f(\delta)$ of packaging cushion material gradually approaches the initial linear, then the response displacement δ is smaller, and the displacement PDF $p_3(\delta)$ is closer to Gaussian distribution with the external excitation intensity decreases.

Assuming $\sigma_0^2 = 0.05, \omega_3 = 1, d_3 = 2, \omega_4 = 2$, and $(k_4/F_4) = 0.1$, the displacement PDFs of ATHNPS can be plotted for various values of damping coefficient α in Figure 16. Damping correlation coefficient α is higher as the cushion capacity of the system increases, and the displacement response is limited to a smaller range. The system damping is considered
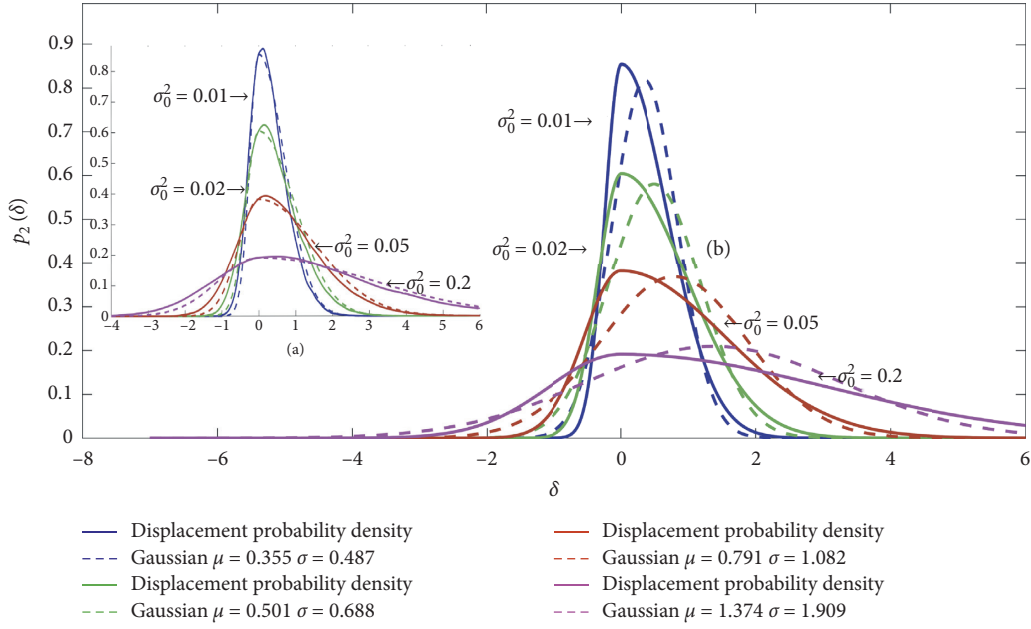
FIGURE 11: Displacement PDFs of AHTNPS for various values of σ_0^2. (a) Comparison of the numerical and theoretical solution. (b) The result of Gaussian fitting.
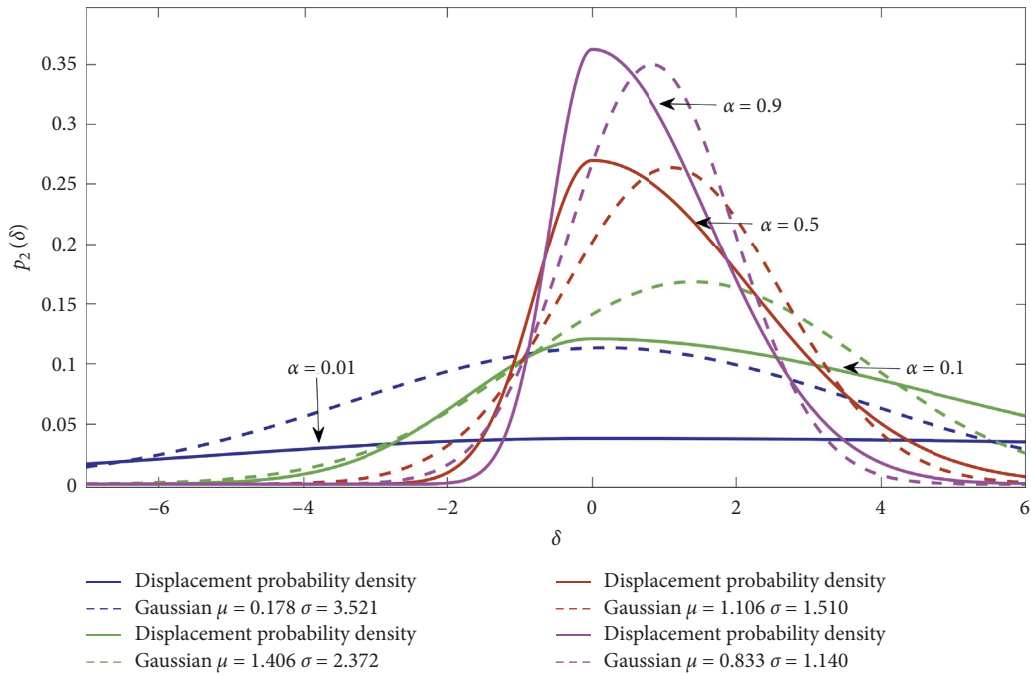

FIGURE 12: Displacement PDFs of AHTNPS for various damping coefficients.

as linear; with the α increases, the nonlinear factors can also be compensated in the system so that $p_3(\delta)$ is closer to Gaussian distribution. It is interesting to find that as α tends to 0 (the system damping tends to 0), $p_3(\delta)$ approaches a uniform distribution.

Letting $n_3 = (4\alpha\omega_3^2 d_3^2/\pi^2\sigma_0^2)$ and $n_4 = (-\alpha F_4\omega_4'^2/k_4'\sigma_0^2)$, equation (16) becomes

$$
p_3(\delta) = \begin{cases} C_1'\left(\cos\dfrac{\pi\delta}{2d_3}\right)^{n_3}, & d_3 \geq \delta \geq 0, n_3 \geq 0, \\[3mm] C_1'\left(\cosh\dfrac{k_4'\delta}{F_4}\right)^{n_4}, & \delta < 0, n_4 \leq 0. \end{cases} \tag{17}
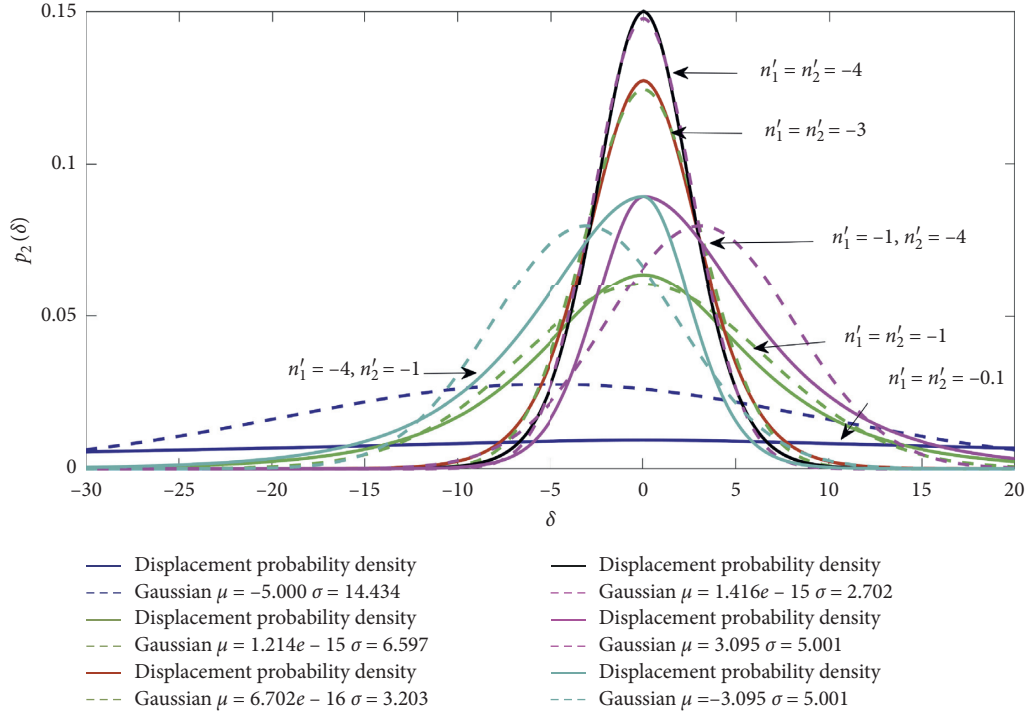$$

FIGURE 13: Displacement PDFs of AHTNPS for various values of n_1' and n_2'.
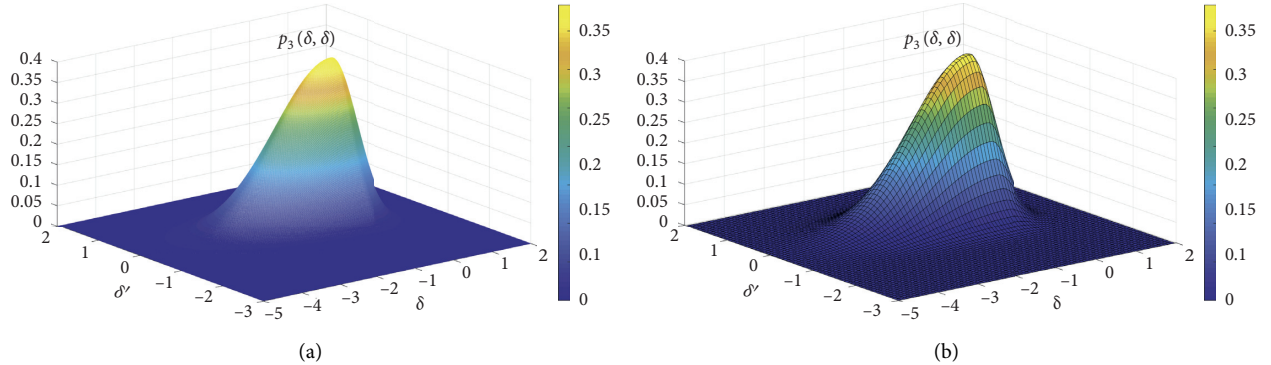

(a)

(b)

FIGURE 14: Comparison of displacement and velocity united PDF of ATHNPO. (a) Theoretical solution. (b) Numerical solution.

When $d_3 = 2$ and $(k_4/F_4) = 0.2$, the amplitude δ is plotted versus displacement PDFs of ATHNPS for various values of n_3 and n_4 in Figure 17. It is interesting to find that as IECFs n_3 and n_4 tending to 0 (σ_0^2 tends to infinity), $p_3(\delta)$ is approaching a uniform distribution. It shows that as (n_3/n_4) following the proportion, $p_3(\delta)$ is approaching the Gaussian distribution, else $p_3(\delta)$ presents non-Gaussian characters. As n_1' and n_2' tend to infinity (σ_0^2 tends to 0), $p_3(\delta)$ can be regarded as Gaussian distribution.

5. Peak PDFs of ANPSs

The times of sample function cross zero with positive slope were given by To [33]:

$$v_0^+ = \int_0^{+\infty} \dot{\delta} p(0, \dot{\delta}) d\dot{\delta}, \tag{18}$$

and after substituting equation (18) into $p(\delta, \dot{\delta})$, zero crossing with positive slope of three packaging system can be obtained.

The displacement peak PDF would like to be known to determine the probability of fatigue failure; it will estimate the relative frequency of occurrence for any peak amplitude. A method to obtain the distribution was suggested by Crandall [34]:

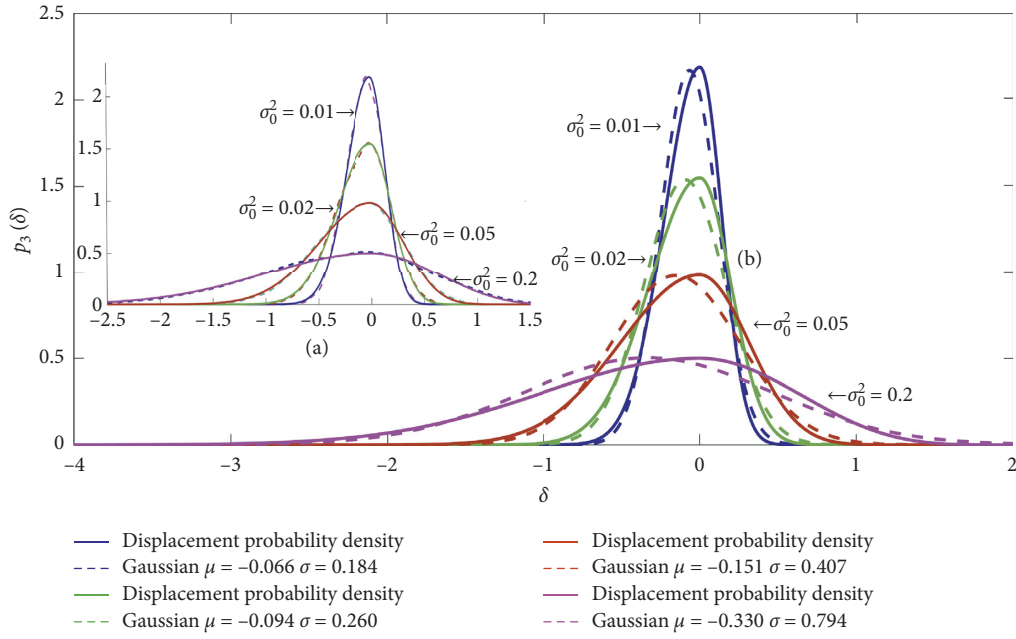$$p_{\text{peak}}(h)dh = -\left(\frac{1}{v_0^+}\right)\left(\frac{dv_h^+}{dh}\right)dh, \tag{19}$$

FIGURE 15: Displacement PDFs of ATHNPS for various values of σ_0^2. (a) Comparison of the numerical and theoretical solution. (b) The result of Gaussian fitting.

generally, v_0^+ only concerns positive numbers by the equation (18), considering $-\delta$ when $\delta < 0$, and combining the equations (19) and (18), we can obtain the generalized peak PDF

$$p_{\text{peak}}(h) = \frac{-[dp(\delta)/d\delta]_{\delta=h}}{p(\delta)_{\delta=0}}. \tag{20}$$

5.1. Peak PDFs of ATNPS. Equation (6) gives

$$p_1(0, \dot{\delta}) = \frac{C_1}{\sqrt{2\pi}\sigma_0} \exp\left[-\left(\frac{\dot{\delta}^2}{2\sigma_0^2}\right)\right], \tag{21}$$

and substituting equation (21) into (18), then

$$v_0^+ = \int_0^{+\infty} \dot{\delta} p(0, \dot{\delta}) d\dot{\delta} = \frac{C_1}{\sqrt{2\pi}\sigma_0} \int_0^{+\infty} \dot{\delta} \exp\left[-\left(\frac{\dot{\delta}^2}{2\sigma_0^2}\right)\right] d\dot{\delta}, \tag{22}$$

and letting $\dot{z}_1 = (\dot{\delta}^2/2\sigma_0^2)$, after integral transform,

$$v_0^+ = \int_0^{+\infty} \dot{\delta} p(0, \dot{\delta}) d\dot{\delta} = -\frac{C_1 \sigma_0^2}{\sqrt{2\pi}} \int_0^{+\infty} \dot{z}_1 \exp(-\dot{z}_1) d\dot{z}_1. \tag{23}$$

Since the integral $\int_0^{+\infty} \dot{z}_1 \exp(-\dot{z}_1) d\dot{z}_1$ is equal to unity, v_0^+ is given as

$$v_0^+ = \frac{-\sigma_0^2 [d_1 \Gamma(n_1 + 1/2)/\Gamma(n_1/2 + 1) + d_2 \Gamma(n_2 + 1/2)/\Gamma(n_2/2 + 1)]}{\sqrt{2\pi}}. \tag{24}$$

Equation (7) yields

$$\frac{dp_1(\delta)}{d\delta} = \begin{cases} -\dfrac{C_1 n_1 \pi}{2d_1}\left(\cos\dfrac{\pi\delta}{2d_1}\right)^{n_1-1}\left(\sin\dfrac{\pi\delta}{2d_1}\right), & 0 \le \delta < d_1, \\[3mm] -\dfrac{C_1 n_2 \pi}{2d_2}\left(\cos\dfrac{\pi\delta}{2d_2}\right)^{n_2-1}\left(\sin\dfrac{\pi\delta}{2d_2}\right), & -d_2 < \delta < 0, \end{cases} \tag{25}$$

then

$$\left[\frac{dp_1(\delta)}{d\delta}\right]_{\delta=h} = \begin{cases} -\dfrac{C_1 n_1 \pi}{2d_1}\left(\cos\dfrac{\pi h}{2d_1}\right)^{n_1-1}\left(\sin\dfrac{\pi h}{2d_1}\right), & 0 \le h < d_1, \\[3mm] -\dfrac{C_1 n_2 \pi}{2d_2}\left(\cos\dfrac{\pi h}{2d_2}\right)^{n_2-1}\left(\sin\dfrac{\pi h}{2d_2}\right), & -d_2 < h < 0, \end{cases} \tag{26}$$

and from equation (7),

$$[p_1(\delta)]_{\delta=0} = C_1 = \frac{\sqrt{\pi}}{[\Gamma(n_1 + 1/2)/\Gamma(n_1/2 + 1) + \Gamma(n_2 + 1/2)/\Gamma(n_2/2 + 1)]}, \qquad n_1 \ge 0, n_2 \ge 0, \tag{27}$$
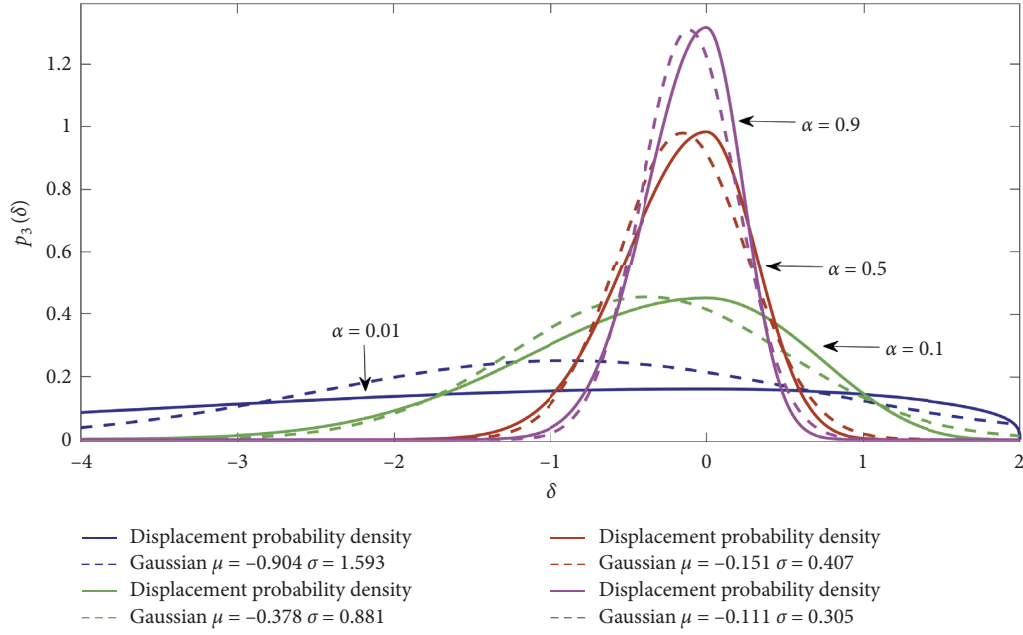
and substituting equations (26) and (27) into (20),

FIGURE 16: Displacement PDFs of ATHNPS for various values of damping coefficient.

$$p_{1peak}(h) = \begin{cases} \dfrac{n_1\pi}{2d_1}\tan\dfrac{\pi h}{2d_1}\left(\cos\dfrac{\pi h}{2d_1}\right)^{n_1}, & 0\le h<d_1, \\[4mm] \dfrac{n_2\pi}{2d_2}\tan\dfrac{\pi h}{2d_2}\left(\cos\dfrac{\pi h}{2d_2}\right)^{n_2}, & -d_2<h<0. \end{cases}$$

(28)

Letting $d_1 = d_2 = (\pi/2)$, the generalized peak PDFs of ATNPS can be displayed for various values of n_1 and n_2 in Figure 18. As the IECFs n_1 and n_2 decrease, the displacement peaks corresponding to the generalized $p_{1peak}(h)$ of the product move lower and wider. Meanwhile, the response displacement peaks of the product present a wider range.

Then, we use Rayleigh, Weibull, and Gaussian distributions to examine the generalized peak PDFs of ATNPS for $h \ge 0$, and the result is also depicted in Figure 18. At this case , $p_{1peak}(h)$ is approaching Rayleigh and Weibull distribution as n_1 and n_2 increase. What's more, $p_{1peak}(h)$ is closer to Rayleigh distribution than Weibull distribution. Figure 18 reveals that as n_1 and n_2 change, $p_{1peak}(h)$ presents non-Gaussian characters.

Generalized peak PDFs of ATNPS can be plotted for different d_1 and d_2 in Figure 19 when $n_1 = 5$ and $n_2 = 5$. As d_1 and d_2 are lower, we can see that the displacement peaks corresponding to the generalized $p_{1peak}(h)$ of the product move higher and narrower. Meanwhile, the response displacement peaks of the product present a narrower range.

Rayleigh, Weibull, and Gaussian distributions are introduced to examine the generalized peak PDFs of ATNPS for $h \ge 0$ for different d_1 and d_2. It is obvious that $p_{1peak}(h)$ is approaching Weibull and Rayleigh distribution from Figure 19 as d_1 and d_2 increase. In addition, $p_{1peak}(h)$ is closer to Rayleigh distribution than Weibull distribution. On the contrary, $p_{1peak}(h)$ is only approaching Rayleigh distribution as d_1 and d_2

decrease. Figure 19 shows that whatever d_1 and d_2 change, $p_{1peak}(h)$ presents non-Gaussian characters.

5.2. Peak PDFs of AHTNPS.

Equation (12) yields

$$p_2(0,\dot\delta) = \frac{C_1'}{\sqrt{2\pi}\sigma_0}\exp\left(\frac{F_1^2\omega_1'^2}{k_1'}\right)\exp\left[-\left(\frac{\dot\delta^2}{2\sigma_0^2}\right)\right],$$

(29)

and substituting equation (29) into (18), letting $\dot z_2 = (\dot\delta^2/2\sigma_0^2)$, after integral transform, then

$$v_0^+ = \int_0^{+\infty}\dot\delta p(0,\dot\delta)\mathrm{d}\dot\delta = \frac{\sqrt{2}C_1'}{\sqrt{\pi}}\int_0^{+\infty}\dot z_2\exp(-\dot z_2)\mathrm{d}\dot z_2.$$

(30)

Since the integral $\int_0^{+\infty}\dot z_2\exp(-\dot z_2)\mathrm{d}\dot z_2$ is equal to unity, v_0^+ is given as $v_0^+ = (\sqrt{2\pi}\,C_1'/\pi)$.

From equation (13), $[\mathrm{d}p_2(\delta)/\mathrm{d}\delta]_{\delta=h}$ can be obtained and $[p_2(\delta)]_{\delta=0} = C_1'$. Substituting above equations into equation (20) result in

$$p_{2peak}(h) = \begin{cases} -\dfrac{k_1'n_1'}{F_1}\tanh\dfrac{k_1'h}{F_1}\left(\cosh\dfrac{k_1'h}{F_1}\right)^{n_1'}, & h\ge 0, n_1'\le 0, \\[4mm] -\dfrac{k_2'n_2'}{F_2}\tanh\dfrac{k_2'h}{F_2}\left(\cosh\dfrac{k_2'h}{F_2}\right)^{n_2'}, & h<0, n_2'\le 0. \end{cases}$$

(31)

Letting $(k_1'/F_1) = (k_2'/F_2) = 1$, the generalized peak PDFs of AHTNPS can be displayed except the difference in n_1' and n_2' in Figure 20. As IECFs n_1' and n_2' decrease, it can be seen that the displacement peaks corresponding to the generalized $p_{2peak}(h)$ of the product move lower and wider. Meanwhile, the response displacement peaks of the product present a wider range.
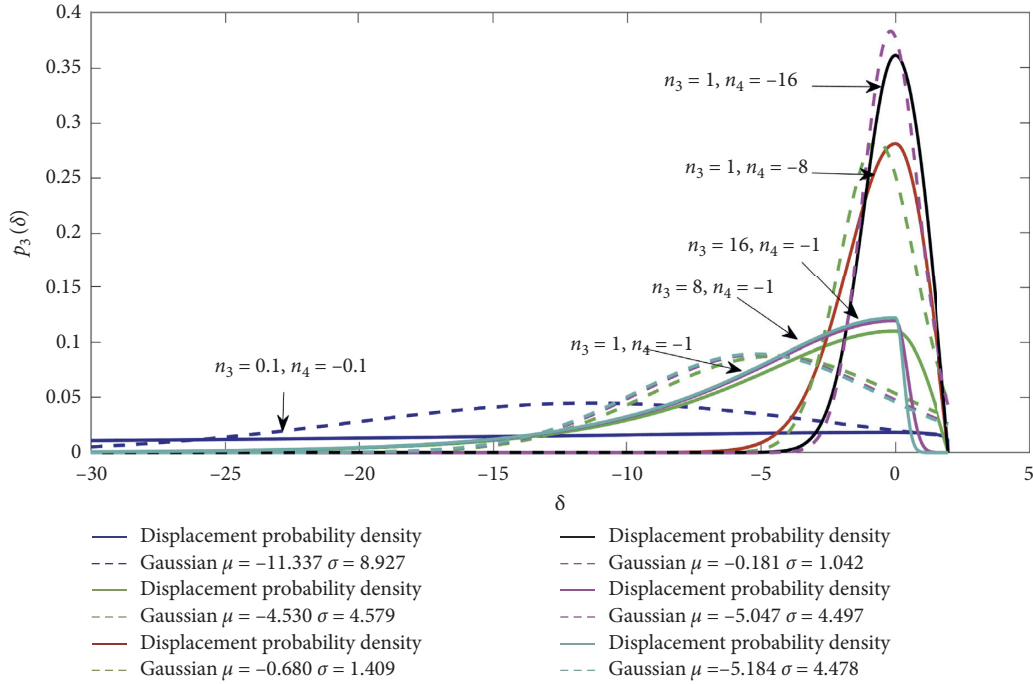
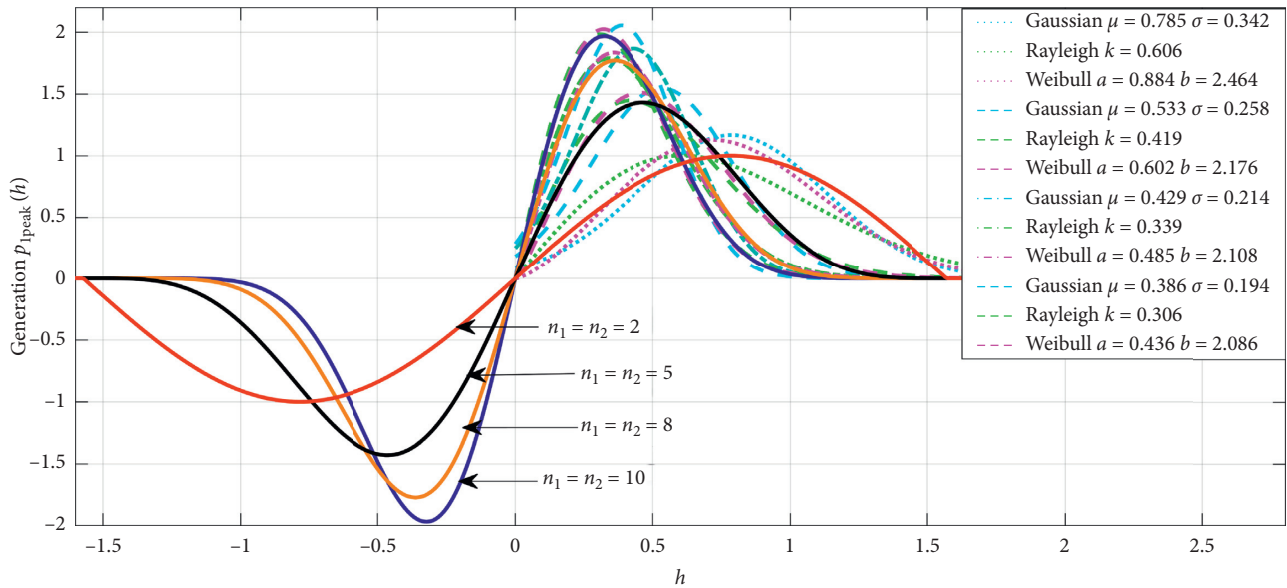FIGURE 17: Displacement PDFs of ATHNPS for various values of n_3 and n_4.

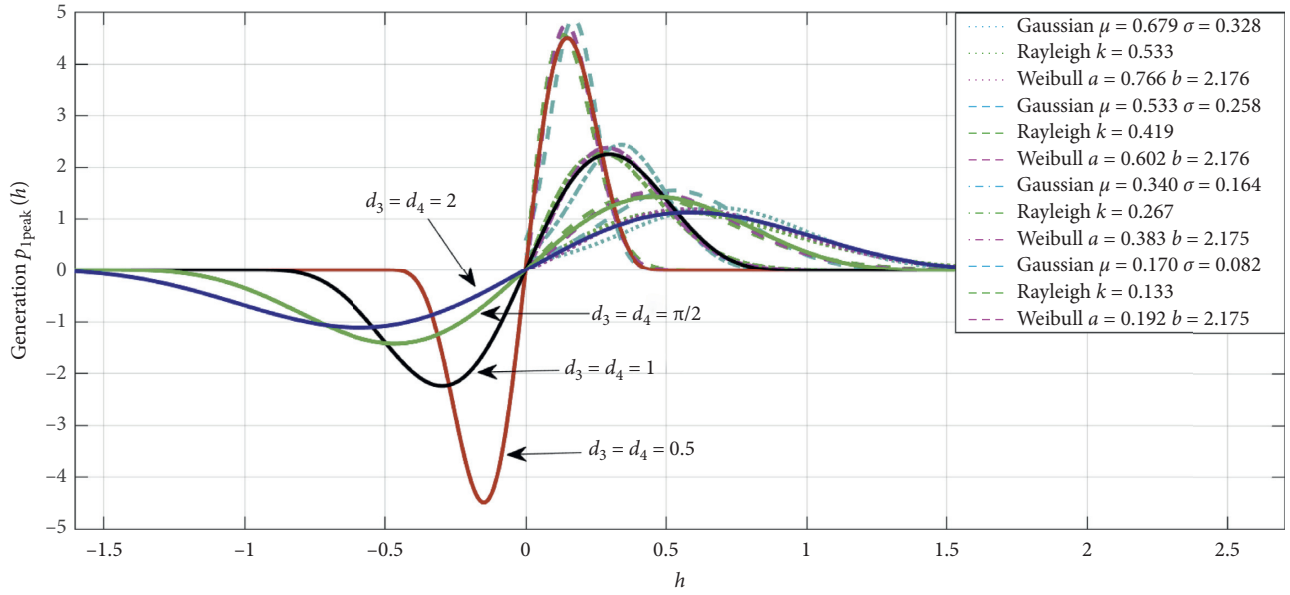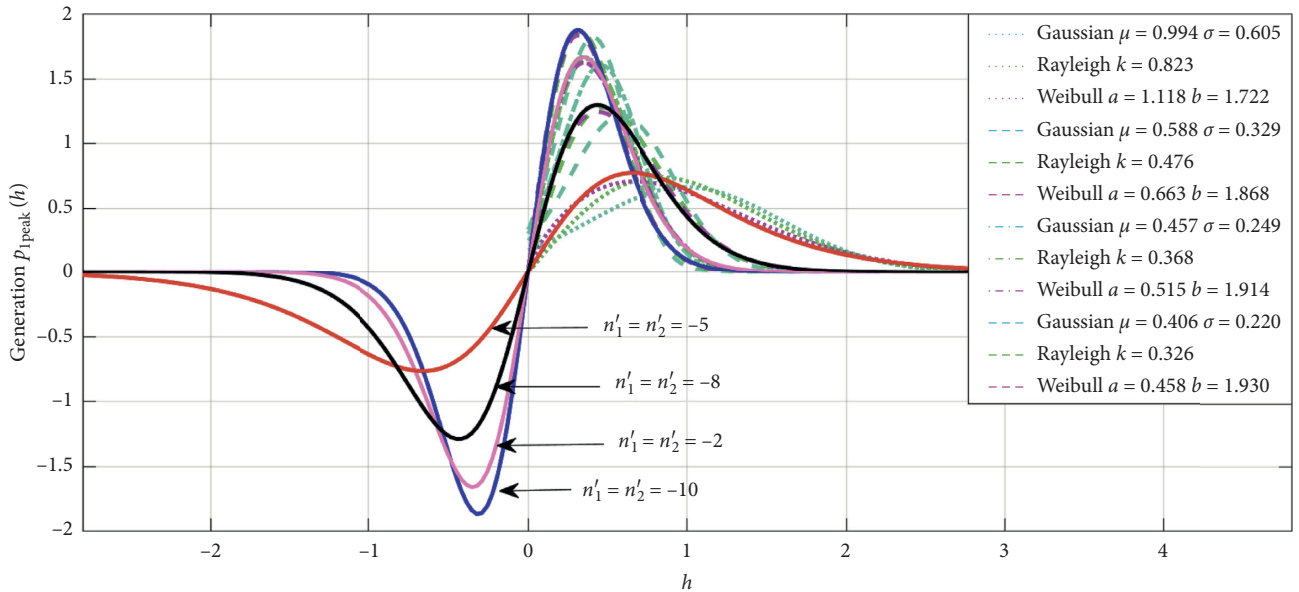FIGURE 18: Generalized peak PDFs of ATNPS for various values of n_1 and n_2.

When $h \geq 0$, the amplitude h is plotted versus the generalized peak PDFs of HATNPO for various n_1' and n_2' in Figure 20. It is shown that $p_{2\text{peak}}(h)$ is approaching Rayleigh and Weibull distribution in Figure 20 as n_1' and n_2' increase. $p_{2\text{peak}}(h)$ is closer to Rayleigh distribution than Weibull distribution. $p_{2\text{peak}}(h)$ approaches Weibull distribution as n_1' and n_2' decrease. Figure 20 indicates that as n_1' and n_2' change, $p_{2\text{peak}}(h)$ presents distinct non-Gaussian characters.

5.3. Peak PDFs of ATHNPS. Equation (16) gives

$$p_3(0, \dot{\delta}) = \frac{C_1^{'}}{\sqrt{2\pi}\sigma_0} \exp\left[-\left(\frac{\dot{\delta}^2}{2\sigma_0^2}\right)\right], \qquad (32)$$

substituting equation (32) into (18), after integral transform, we can also obtain $v_0^+ = (-C_1'\sigma_0^2/\sqrt{2\pi})$.

Based on the equations (17) and (20), we can obtain

FIGURE 19: Generalized peak PDFs of ATNPS for different d_1 and d_2.

FIGURE 20: Generalized peak PDFs of AHTNPS except the difference in n_1' and n_2'.

$$p_{3\text{peak}}(h) = \begin{cases} \dfrac{n_3\pi}{2d_3}\left(\tan\dfrac{\pi h}{2d_3}\right)\left(\cos\dfrac{\pi h}{2d_3}\right)^{n_3}, & 0 \le h < d_3, n_3 \ge 0, \\[4mm] -\dfrac{k_4 n_4}{F_4}\left(\tanh\dfrac{k_4 h}{F_4}\right)\left(\cosh\dfrac{k_4 h}{F_4}\right)^{n_4}, & h < 0, n_4 \le 0. \end{cases}$$

(33)

Letting $d_3 = (\pi/2)$, $(k_4/F_4) = 1$, the generalized peak PDFs of ATHNPS can be displayed for various values of n_3 and n_4 in Figure 21. With the IECF n_3 increases and n_4 decreases, we can see that the displacement peak h corresponding to the generalized $p_{3\text{peak}}(h)$ of the product moves

lower and wider. Meanwhile, the response displacement peak h of the product presents a wider range.

When $h \ge 0$, the amplitude h is plotted versus generalized peak PDFs of ATNPS for various values of n_3 and n_4 also in Figure 21. It is shown that $p_{3\text{peak}}(h)$ is approaching Rayleigh as n_3 increases and n_4 decreases. Figure 21 indicates that as n_3 and n_4 change, $p_{3\text{peak}}(h)$ presents non-Gaussian characters.

6. Application for Fatigue Evaluation

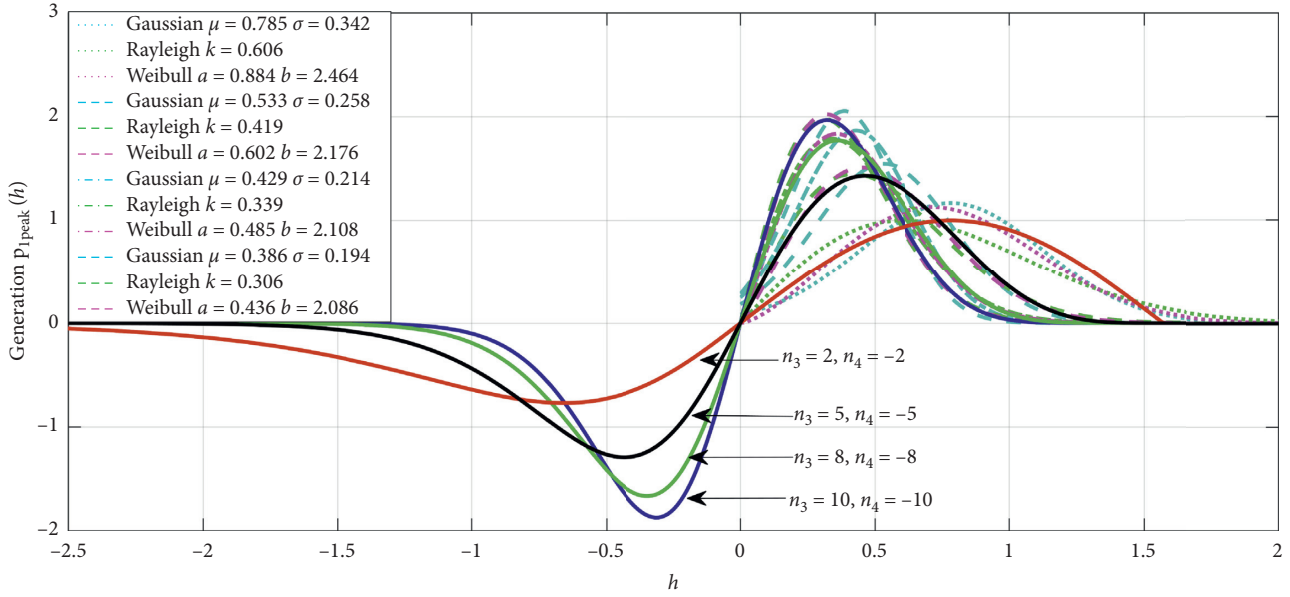Some rocket component packaged by the neoprene and some foam alloy composite materials of the aircraft are

FIGURE 21: Generalized peak PDFs of ATHNPS for various values of n_3 and n_4.
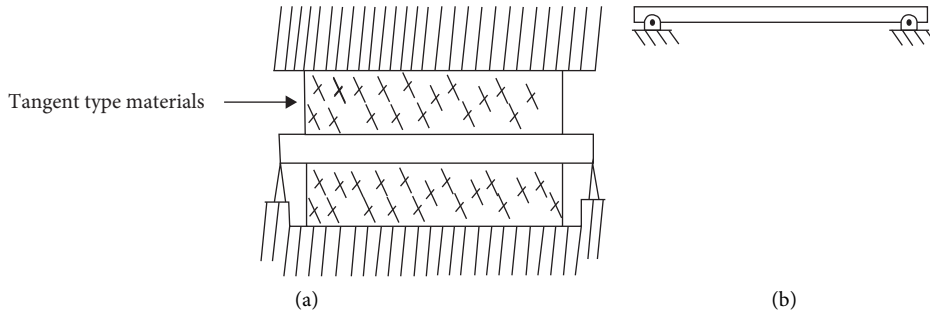

FIGURE 22: Displacement nonlinearity due to tangent type materials.

subjected to the random loading during the air transport so as to cause the fatigue failure.

Take ATNPO as example shown in Figure 22, assuming that fatigue damage accumulates linearly (Miner's rule) [35], the average damage $E(D)$ after N_1 cycles was given by [36]:

$$E(D) = N_1\mu \int_0^\infty s^\beta p(s)\mathrm{d}s, \tag{34}$$

where μ is a constant of any given material, β is the slope of the $s - N$ curve by the logarithmic coordinate, and $p(s)$ represents the PDF of peak stress amplitude, which can be obtained through the generalized PDF of the response peak distribution $p_{\mathrm{peak}}(h)$.

(a) The system under study can be regarded as an approximate motion description at the center of a simply supported beam in Figure 22(a), so the stress-displacement relationship can be assumed linear

$s_1 = \mu_1 h$. Combining equations (31) and (34) results in

$$E(D) = \frac{N_1\mu n\pi}{2\mu_1 d} \int_0^{\mu_1 d} s_1^\beta \tan\frac{\pi s_1}{2\mu_1 d}\left(\cos\frac{\pi s_1}{2\mu_1 d}\right)^n \mathrm{d}s_1, \tag{35}$$

for $\beta \approx 10$ and $n = 9$, solving the integration, equation (35) results in

$$E[D]_{n=9} = \left[0.153 \times 10^{-3}\mu\left(\mu_1 d\right)^9\right]N_1, \tag{36}$$

and if the ultimate strength of a material is 50 000 psi, μ_1 is 25 000 psi/in, and $d = 1$. Equation (36) becomes

$$E[D]_{n=9} = \left[0.153 \times 10^{-3} \times \left(\frac{25000}{500000}\right)^9\right]N_1$$

$$= 2.988 \times 10^{-7}N_1. \tag{37}$$

When $E(D) = 1$, the fatigue failure occurs, so the average cycle number to failure would be $N_a = (1/2.988 \times 10^{-7}) = 3.346 \times 10^6$ cps.

(b) Considering the stress at the center of a pinned-pinned beam shown in Figure 22(b), the stress-displacement nonlinear relationship was given [37] $s_2 = \mu_2 h + (\mu_3'/2l\sqrt{3})h^2 = \mu_2 h + \mu_3 h^2$ (where l represents the length of the beam), and then $h = (-\mu_2 + (\mu_2^2 + 4\mu_3 s_2)^{1/2}/2\mu_3)$ result in

$$E_N(D) = \frac{N_1 \mu n \pi}{2d} \int_0^d s_2^\beta \tan \frac{\pi h}{2d} \left(\cos \frac{\pi h}{2d} \right)^n \mathrm{d}h. \qquad (38)$$

Similarly, $E_N(D)$ and the average cycle number to failure N_a can also be evaluated at some determine parameters.

7. Conclusions

The displacement PDFs of three types of ANPSs have been derived through FPK equations; the generalized peak PDFs are defined and examined by three common distributions. Meanwhile, a good agreement is achieved between theoretical solutions and numerical results, leading to verify the theories. The conclusions lie in the following aspects.

(a) The responses for three types of ANPSs derived through FPK equations present different forms, but they have the generalities. The displacement PDFs for three ANPSs are closer to Gaussian distribution with the external excitation grade decreases.

(b) With the damping correlation coefficient α increases, the nonlinear factors can be compensated in the system, and the displacement PDFs for three types of ANPSs are closer to Gaussian distribution. It is interesting to find that as α tends to 0 (the system damping tends to 0), the displacement PDF approaches the uniform distribution. Displacement responses of asymmetric tangent type are limited to the boundary strain of d_1 and d_2. IECFs have a significance on effecting the displacement PDFs approaching a uniform distribution, non-Gaussian distribution, or Gaussian distribution.

(c) Most PDFs of the unilateral response peaks approach Rayleigh distributions, and present non-Gaussian characters. The application of the scheme for fatigue evaluation is carried out, so the analysis can be used as guidelines for fatigue damage evaluation of the transport package or the critical component.

Data Availability

The data used to support the findings of this study are included within the article.

Conflicts of Interest

The authors declare that they have no conflicts of interest.

References

[1] R. D. Mindlin, "Dynamics of package cushioning," *Bell System Technical Journal*, vol. 24, no. 3, pp. 353–461, 1945.

[2] R. A. Ibrahim, "Recent advances in nonlinear passive vibration isolators," *Journal of Sound and Vibration*, vol. 314, no. 3-5, pp. 371–452, 2008.

[3] J. Wang, F. Duan, J.-H. Jiang, L.-X. Lu, and Z.-W. Wang, "Dropping damage evaluation for a hyperbolic tangent cushioning system with a critical component," *Journal of Vibration and Control*, vol. 18, no. 10, pp. 1417–1421, 2012.

[4] K. Peleg, "Dynamic restoring and dissipative parameters of non-linear systems," *International Journal of Mechanical Sciences*, vol. 23, no. 10, pp. 595–606, 1981.

[5] Z. Wang, C. Wu, and D. Xi, "Damage boundary of a packaging system under rectangular pulse excitation," *Packaging Technology and Science*, vol. 11, no. 4, pp. 189–202, 1998.

[6] Z.-W. Wang and C.-Y. Hu, "Shock spectra and damage boundary curves for non-linear package cushioning systems," *Packaging Technology and Science*, vol. 12, no. 5, pp. 207–217, 1999.

[7] J. Wang, Y. Khan, L. X. Lu, and Z. W. Wang, "Inner resonance of a coupled hyperbolic tangent nonlinear oscillator arising in a packaging system," *Applied Mathematics and Computation*, vol. 218, no. 15, pp. 7876–7879, 2012.

[8] T. K. Caughey, "On the response of non-linear oscillators to stochastic excitation," *Probabilistic Engineering Mechanics*, vol. 1, no. 1, pp. 2–4, 1986.

[9] M. A. Sek and V. Rouillard, "Application of frequency domain analysis in the testing of packages," *Packaging Technology and Science*, vol. 6, no. 1, pp. 3–12, 1993.

[10] B. G. Korenev and L. M. Reznikov, *Dynamic Vibration Absorbers: Theory and Technical Applications*, John Wiley & Sons, Hoboken, NJ, USA, 1993.

[11] Z.-W. Wang and L.-J. Wang, "On accelerated random vibration testing of product based on component acceleration RMS-life curve," *Journal of Vibration and Control*, vol. 24, no. 15, pp. 3384–3399, 2017.

[12] A. Hosoyama, K. Tsuda, and S. Horiguchi, "Development and validation of kurtosis response spectrum analysis for anti-vibration packaging design taking into consideration kurtosis," *Packaging Technology and Science*, vol. 33, no. 2, pp. 1–14, 2019.

[13] R. C. Rountree and F. B. Safford, "Methodology and standardization for fragility evaluation," *Shock and Vibration Bulletin*, vol. 41, no. 5, pp. 111–128, 1970.

[14] K. P. Thakur and D. Pang, "Simulating complex loading patterns in the stack of packages," in *Proceedings of the 10th IAPRI World Conference on Packaging*, pp. 1–12, Melbourne, Australia, March 1997.

[15] B. F. Song, "An approach to the definition and application of the vibrating fragility value," *Package Engineering*, vol. 17, no. 2, pp. 1–5, 1995, in Chinese.

[16] J. P. Liaudet and E. Rigaud, "Experiments and numerical results on non-linear vibrations of an impacting Hertzian contact. part 2: random excitation," *Journal of Sound and Vibration*, vol. 265, no. 2, pp. 309–327, 2003.

[17] C. B. Gan, "Stochastic averaging of packaging oscillatory system under stochastic excitation," *Package Engineering*, vol. 26, no. 5, pp. 18–20, 2005, in Chinese.

[18] L. J. Wang and Z. W. Wang, "Fatigue failure and $G_{rms} - N$ curve of corrugated paperboard box," *Journal of Vibration and Control*, vol. 26, no. 11-12, pp. 1028–1041, 2020.

[19] Y. Y. Chen and C. M. Chen, "Random vibration of a piecewise linear single-degree-of-freedom system (in Chinese)," *Journal of Northeast Engineering Institute*, vol. 35, no. 2, pp. 82–93, 1983.

[20] B. Z. Zhuang, N. L. Chen, B. Fu, and Z. Gao, "The response analysis of several, nonlinear isolation systems subjected to random excitation," *Applied Mathematics and Mechanics (English Edition)*, vol. 7, no. 2, pp. 118–123, 1986.

[21] B. Z. Zhuang, N. L. Chen, B. Fu, and Z. Gao, "Random vibration of an asymmetric nonlinear system with one degree of freedom," *Journal of Applied Mechanics*, vol. 2, no. 1, pp. 127–134+170, 1985, in Chinese.

[22] T. J. Urbanik, "Force plate for corrugated container vibration tests," *Journal of Testing and Evaluation*, vol. 18, no. 5, pp. 359–362, 1990.

[23] X. J. Yang and C. B. Gan, "A study on piecewise linear transit packaging oscillatory system," *Package Engineering*, vol. 25, no. 3, pp. 43–45, 2004, in Chinese.

[24] K. Fang, *Random Vibration Analysis for Stacked Packaging and Monitoring System for Logistics Environment*, Univ. of Jinan, Guangzhou, China, 2018.

[25] K. Fang and Z.-W. Wang, "Influence of jumping phenomenon on response of package under random vibration," *Packaging Technology and Science*, vol. 31, no. 9, pp. 585–599, 2018.

[26] J. Wang, Z.-W. Wang, L.-X. Lu, Y. Zhu, and Y.-G. Wang, "Three-dimensional shock spectrum of critical component for nonlinear packaging system," *Shock and Vibration*, vol. 18, no. 3, pp. 437–445, 2011.

[27] R. H. Huan, R. C. Hu, D. Pu, and W. Q. Zhu, "Optimal vibration control of a class of nonlinear stochastic systems with Markovian jump," *Shock and Vibration*, vol. 2015, Article ID 9641075, 9 pages, 2016.

[28] J. Xue, Y. Zhang, H. Ding, and L. Chen, "Vibration reduction evaluation of a linear system with a nonlinear energy sink under a harmonic and random excitation," *Applied Mathematics and Mechanics*, vol. 41, no. 1, pp. 1–14, 2020.

[29] N. Metropolis, A. W. Rosenbluth, M. N. Rosenbluth, A. H. Teller, and E. Teller, "Equation of state calculations by fast computing machines," *The Journal of Chemical Physics*, vol. 21, no. 6, pp. 1087–1092, 1953.

[30] W. K. Hastings, "Monte Carlo sampling methods using Markov chains and their applications," *Biometrika*, vol. 57, no. 1, pp. 97–109, 1970.

[31] B. Tang, S. B. Wang, M. J. Brennan, L. Feng, and W. Chen, "Identifying the stiffness and damping of a nonlinear system using its free response perturbed with Gaussian white noise," *Journal of Vibration and Control*, vol. 26, no. 9-10, pp. 830–839, 2019.

[32] B. O. Pierce and R. M. Foster, *A Short Table of Integrals*, Ginn & Co., Inc., Boston, MA, USA, 1956.

[33] C. W. S. To, *Nonlinear Random Vibration: Analytical Techniques and Applications*, CRC Press, London, UK, 2011.

[34] S. H. Crandall, "Random vibration of a nonlinear system with a set-up spring," *Journal of Applied Mechanics*, vol. 29, no. 3, pp. 477–482, 1962.

[35] Y.-P. Shen, S.-L. Wang, X.-J. Li, and B. S. Dhillon, "Multiaxial fatigue life prediction of kiln roller under axis line deflection," *Applied Mathematics and Mechanics*, vol. 31, no. 2, pp. 205–214, 2010.

[36] S. H. Crandall, "Zero crossings, peaks, and other statistical measures of random responses," *The Journal of the Acoustical Society of America*, vol. 35, no. 11, pp. 1693–1699, 1963.

[37] P. W. Smith, "Calculations of random fatigue of hard-spring resonators," *The Journal of the Acoustical Society of America*, vol. 33, no. 6, pp. 752–756, 1961.